JGP Journal of General Physiology

ARTICLE

Excitation–Contraction Coupling

Nerve-dependent distribution of subsynaptic type 1 inositol 1,4,5-trisphosphate receptor at the neuromuscular junction

Pompeo Volpe[1], Alessandra Bosutti[2], Alessandra Nori[1], Riccardo Filadi[1,3], Gaia Gherardi[1], Gabor Trautmann[4], Sandra Furlan[3], Gabriele Massaria[2], Marina Sciancalepore[2], Aram Megighian[1], Paola Caccin[1], Annalisa Bernareggi[2], Michele Salanova[4,5], Roberta Sacchetto[6], Dorianna Sandonà[1], Paola Pizzo[1,3], and Paola Lorenzon[2]

Inositol 1,4,5-trisphosphate receptors (IP_3Rs) are enriched at postsynaptic membrane compartments of the neuromuscular junction (NMJ), surrounding the subsynaptic nuclei and close to nicotinic acetylcholine receptors (nAChRs) of the motor endplate. At the endplate level, it has been proposed that nerve-dependent electrical activity might trigger IP_3-associated, local Ca^{2+} signals not only involved in excitation–transcription (ET) coupling but also crucial to the development and stabilization of the NMJ itself. The present study was undertaken to examine whether denervation affects the subsynaptic IP_3R distribution in skeletal muscles and which are the underlying mechanisms. Fluorescence microscopy, carried out on in vivo denervated muscles (following sciatectomy) and in vitro denervated skeletal muscle fibers from flexor digitorum brevis (FDB), indicates that denervation causes a reduction in the subsynaptic IP_3R1-stained region, and such a decrease appears to be determined by the lack of muscle electrical activity, as judged by partial reversal upon field electrical stimulation of in vitro denervated skeletal muscle fibers.

Introduction

Motor innervation is required for the maturation and maintenance of diversity of both slow-twitch and fast-twitch fibers, thus regulating the contractile properties of skeletal muscle fibers, in part through the effect of electrical activity on the expression of distinct myosins. Motor innervation is also required for the attainment and maintenance of trophic homeostasis and muscle mass (Tintignac et al., 2015), with inactivity and denervation being paramount causes of skeletal muscle atrophy (Carlson, 2014).

Efficient neuromuscular transmission requires complex machineries both at pre- and postsynaptic compartments of the neuromuscular junction (NMJ). The motorneuron has developed molecular strategies to tune the adequate release of neurotransmitter acetylcholine (ACh); the skeletal muscle fiber has adopted strategies to maximize the binding of ACh to nicotinic acetylcholine receptors (nAChRs) to trigger action potentials and to turn on the excitation–contraction (EC) coupling apparatus.

Expression, distribution, and stability of nAChR at the endplate are controlled by both the release of soluble factors from motor nerve endings and the electrical activity of muscle fibers (Duclert and Changeux, 1995; Missias et al., 1996; Sanes and Lichtman, 2001; Li et al., 2018; Shi et al., 2012). Skeletal muscle denervation causes nAChR cluster dispersal at the endplate zone, reduction in the half-life of synaptic nAChRs, and isoform switch from adult ε-nAChRs to embryonic γ-nAChRs, the latter being diffusely distributed over the muscle plasma membrane (Midrio, 2006; Wu et al., 2014).

Among nerve-derived chemical messengers, a key role is played by the proteoglycan agrin (McMahan, 1990) via the activation of the Lrp4/MuSK receptor complex (Li et al., 2018).

[1]Department of Biomedical Sciences and Interdepartmental Research Center of Myology (cirMYO), University of Padova, Padova, Italy; [2]Department of Life Sciences, University of Trieste, Trieste, Italy; [3]National Research Council, Neuroscience Institute, Padova, Italy; [4]Charité-Universitätsmedizin Berlin, Corporate Member of Freie Universität Berlin, Humboldt-Universität zu Berlin and Berlin Institute of Health, Institute of Integrative Neuroanatomy, Berlin, Germany; [5]Neuromuscular Signaling, Center of Space Medicine Berlin, Berlin, Germany; [6]Department of Comparative Biomedicine and Food Science, University of Padova, Padova, Italy.

Correspondence to Pompeo Volpe: pompeo.volpe@unipd.it

This work is part of a special issue on excitation–contraction coupling.

Neural agrin controls the growth and stabilization of the endplate nAChRs (Sanes and Lichtman, 2001) and the distribution and expression of a number of other components of the postsynaptic apparatus (Wallace, 1989; Meier et al., 1997; Briguet and Ruegg, 2000).

As to the regulating effect of the electrical activity, direct muscle stimulation alone is able to prevent the denervation effects at the endplate level. In denervated active/stimulated muscles, electrical activity prevents the denervation-induced decline of metabolic nAChR stability and the loss of endplate structure, and also suppresses the expression of the fetal γ-nAChRs (Brenner and Rudin, 1989). Moreover, direct muscle stimulation counteracts the reduction in the endplate nAChR density induced by blockade of the neuromuscular transmission (Akaaboune et al., 1999). The effects of the induced electrical activity are mediated by an increase in intracellular Ca^{2+} concentration ($[Ca^{2+}]_i$), through either ligand-gated, L-type channels or intracellular Ca^{2+} stores, and are, at least in part, dependent on nAChRs phosphorylation (Martinez-Pena y Valenzuela and Akaaboune, 2021).

The electrical activity of muscle fibers also exerts its role by changes in $[Ca^{2+}]_i$, definitely unrelated to RyR-Ca^{2+} channels responsible for Ca^{2+} release from the SR during EC coupling (Ríos and Pizarro, 1991): evidence is accruing in favor of an inositol 1,4,5-trisphosphate receptor (IP_3R)-mediated Ca^{2+} signaling in the activity-dependent regulation of muscle gene expression (Araya et al., 2003), a process referred to as excitation–transcription (ET) coupling, through which skeletal muscle fibers decode the motoneuron stimulation pattern into a specific gene expression profile and phenotype (Casas et al., 2022).

The presence of all the intermediate steps involved in the metabolism of phosphoinositides, from synthesis to degradation of IP_3 (Milani et al., 1988; Hidalgo and Jaimovich, 1989), the presence of IP_3Rs, as shown by in situ hybridization, immunohistochemistry, and $[^3H]$-IP_3 binding (Moschella et al., 1995), provides a role for IP_3 in skeletal muscle function highly likely (Volpe et al., 1985; Vergara et al., 1985), although unrelated to proposals concerning the role of IP_3 as a chemical messenger for EC coupling (Somlyo, 1985; Blaauw et al., 2012).

IP_3R immunofluorescence analysis shows a staining pattern indicative of the localization of IP_3Rs at the Z-line in murine muscles different from that of type 1 RyRs. In addition, subcellular fractionation experiments show IP_3R to be enriched in longitudinal SR but not in terminal cisternae containing RyRs (Salanova et al., 2002; Powell et al., 2003). IP_3Rs are also enriched at postsynaptic components of the NMJ, surrounding the subsynaptic nuclei and close to nAChRs of the motor endplate (Powell et al., 2003). At the endplate level, IP_3R1 is the prevalent isoform and is involved in synaptic gene expression, as determined by RNA interference-mediated IP_3R1 gene silencing (Zhu et al., 2011). IP_3R1s could be placed either in walls of the synaptic folds, subsynaptic triads (Dauber et al., 2000), and/or junctions of unknown function between subsynaptic folds and rough SR (Dauber et al., 1999).

Nerve-driven electrical activity might trigger IP_3-associated, local Ca^{2+} signals in NMJ involved not only in gene regulation but also crucial to the development and stabilization of the NMJ itself (Powell et al., 2003). In more detail, a functional interplay between nAChRs activity and IP_3R1-driven Ca^{2+} release has been proposed to be responsible for localized subsynaptic Ca^{2+} signaling (Zayas et al., 2007; Zhu et al., 2011). In pathophysiological conditions, abnormal activity of IP_3Rs could also be responsible for Ca^{2+} overload observed in the slow-channel myasthenic syndrome (Zayas et al., 2007) and for NMJ degeneration during excessive cholinergic activation (Zhu et al., 2011).

Although hypotheses have been formulated for the presence and role of subsynaptic IP_3R-driven Ca^{2+} signaling in innervated skeletal muscle fibers, it is not known whether and how innervation controls the subsynaptic IP_3R1 membrane compartment. Based on the significant rearrangement of the endplate region following denervation and the supposed functional interaction between endplate nAChRs and IP_3R1s, the present study was undertaken to examine whether denervation affects the subsynaptic IP_3R1 distribution and to unveil the mechanisms controlling the expression and localization of subsynaptic IP_3R1s. Fluorescence microscopy carried out on in vivo denervated muscles (sciatectomy) and in vitro denervated adult skeletal muscle fibers (cultured flexor digitorum brevis [FDB] muscle fibers) indicates that denervation caused a reduction in the subsynaptic IP_3R1-stained region and that such a decrease appeared to be determined mainly by the lack of muscle electrical activity.

Materials and methods

Animals

Wistar rats and C57BL/6 mice were housed in certified animal facilities at the Universities of Padova and Trieste, respectively, in a 12-h light/12-h dark cycle, bred, and fed ad libitum within the guidelines and rules of the European legislation (2010/63/EU).

In vivo denervation procedure

6-wk-old female Wistar rats (140–160 g of body weight) were anesthetized before surgery and were treated with antibiotics and pain reliever drugs after surgery, as specified in *Aut. Min.* 1089-2020. Denervation procedure, i.e., sciatectomy, was performed on the right leg as previously described (Bortoloso et al., 2006) according to the recommendations provided by the European Convention for the Protection of Vertebrate Animals used for Experimental and Scientific Purposes (Council of Europe No. 123, Strasbourg, 1985) and authorized by the Animal Care Committee of the University of Padova and the Italian Health Ministry, in agreement with the European legislation (2010/63/EU), as per *Aut. Min.* 1089-2020. 9 d after sciatectomy, rats were sacrificed and extensor digitorum longus (EDL) muscles were dissected from both left (contralateral, control) and right (denervated) legs.

Isolation of adult skeletal muscles fibers

Single adult skeletal muscle fibers were obtained from the dissociation of FDB muscles of 6–8-wk-old C57BL/6 male mice (20–25 g of body weight). Mice were sacrificed by cervical

dislocation as approved by the local Animal Care Committee of the University of Trieste and the Italian Health Ministry, in agreement with the European legislation (2010/63/EU).

FDB muscle fibers were isolated from both hindlimb foot muscles of a single mouse for each independent preparation. Immediately after excision, FDB muscles were treated with type I collagenase 0.3% (*w*/*v*; Sigma-Aldrich) for 1 h in ice and 1 h at 37°C in Tyrode's solution containing (in mM) 137 NaCl, 2.7 KCl, 1 $MgCl_2$, 1.8 $CaCl_2$, 0.35 Na_2HPO_4, 12 $NaHCO_3$, 25.5 HEPES, and 5.5 *D*-glucose, pH 7.4 NaOH, plus 100 U/ml penicillin, 100 µg/ml streptomycin, and 10% FBS (Gibco). Single fibers (750–900 for each mouse) were isolated by mechanical dissociation with Pasteur pipettes with decreasing tip diameters and allowed to settle on Matrigel-coated (1 mg/ml; Corning) glass coverslips in 35-mm Petri dishes.

In vitro denervation of adult skeletal muscle fibers

Denervation effects at the endplate region were induced in vitro (Grohovaz et al., 1993) by culturing single adult FDB muscle fibers for up to 7 d in a medium composed of DMEM high glucose enriched (Sigma-Aldrich) supplemented with horse serum (5%; Gibco), *L*-glutamine (2 mM), penicillin (100 IU/ml), and streptomycin (100 µg/ml) at 37°C in a 100% humid air atmosphere containing 5% CO_2. The medium was renewed every 3 d. In these experimental conditions, progressive disarray of the endplate and the appearance of the fetal γ-nAChR isoform occurred after in vivo denervation (Henderson et al., 1987; Tarpey et al., 2018; Gupta et al., 2020). According to the experimental purposes, cultures were maintained in Tyrode's solution at 37°C in a 100% humid air atmosphere containing 5% CO_2 (control conditions) or underwent specific treatments (neural agrin exposure or field electrical stimulation; see below).

Neural agrin treatment of adult, cultured skeletal muscle fibers

The addition of 1 nM recombinant C-terminal fragment of rat agrin-z^+ (550-AG; R&D Systems) to the culture medium started 24 h after dissociation. Each experimental point was obtained from skeletal muscle fibers isolated from the same animal and cultured in the absence (control) or the presence of neural agrin. Renewal of the medium was performed every 3 d and 1 nM neural agrin was added, where applicable, at each medium change.

Field electrical stimulation of adult, cultured skeletal muscle fibers

The effect of field electrical stimulation was analyzed by comparing adult skeletal muscle fibers isolated from the same animal, cultured at 37°C in a 100% humid air atmosphere containing 5% CO_2 in the absence (control) and the presence of electrical stimulation. Electrical stimulation was delivered to muscle fibers using a Grass S88 stimulator (Grass Instruments). The stimulator was connected to a device constituted by a 6-well plate with two connection cards associated with two parallel platinum–iridium electrodes (0.2 mm in diameter) in each well, placed 2 cm apart and positioned 1–2 mm over the cells. Field electrical stimulation was performed daily, for 5 h, and started from 24 h after dissociation. Capacitors in series with the electrodes allowed the delivery of biphasic single pulses of 1 ms width at a frequency of 1 Hz. The medium was renewed every 3 d.

nAChR and IP_3R1 staining

EDL muscles from controlateral and denervated hindlimbs of each rat were dissected and rapidly frozen in liquid nitrogen. Processing and staining were carried out on 30-µm longitudinal cryosections postfixed with 4% (w/v) paraformaldehyde in PBS for 45 min at room temperature, then blocked with 10% goat serum in PBS (v/v) supplemented with Triton-X100 0.3% (v/v), followed by incubation for 48 h at 4°C with polyclonal antibodies against IP_3R1s (1:250 in PBS, PA3-901A; Thermo Fisher Scientific Life Sciences) or antibodies raised against a synthetic peptide corresponding to IP_3R1 aa 1829–1848 developed by Volpe et al. (1993). Sections were extensively washed in PBS and stained with goat anti-rabbit IgG–Alexa Fluor 488 conjugated secondary antibodies (1:500 in PBS; A11034; ThermoFisher Scientific Life Sciences) together with 2 µg/ml snake toxin α-bungarotoxin (α-BuTX) Alexa Fluor 555 conjugate (B35451; ThermoFisher Scientific Life Sciences) overnight. After the secondary antibodies and the toxin were removed, slides were washed three times and mounted using Pro Long antifade with DAPI mounting medium (Thermo Fisher Scientific Life Sciences).

In single FDB muscle fibers, nAChRs and IP_3R1s labeling was carried out from 24 h up to 7 d after dissociation. Fixation was carried out on coverslips with a solution of 4% (w/v) paraformaldehyde in PBS for 15 min at 4°C. Fibers were then permeabilized in PBS + Triton-X100 0.3% (v/v) for 15 min and incubated in a blocking solution containing PBS plus 2% BSA (Sigma-Aldrich) for 30 min. IP_3R1s were stained with either rabbit polyclonal anti-IP_3R1s antibodies PA3-901A (Thermo Fisher Scientific Life Sciences) or antibodies developed by Volpe et al. (1993). Rabbit polyclonal anti-IP_3R1s antibodies were diluted 1:100 in blocking solution, and cell incubation was performed overnight at 4°C. Muscle fibers were incubated for 1 h at room temperature with the secondary goat anti-rabbit Alexa Fluor 568 conjugated antibody (1:500 in PBS; A11036; Thermo Fisher Scientific Life Sciences) and Hoechst solution (1:2,000 in PBS; Thermo Fisher Scientific Life Sciences). nAChRs were labeled by 2.5 µg/ml Alexa Fluor 488–α-BuTX in PBS supplemented with 0.1% BSA (v/v) for 1 h at room temperature. After staining, fibers were washed three times with PBS and finally rinsed with distilled water and mounted on a microscope glass.

Analysis of nAChR and IP_3R1 staining

In single FDB muscle fibers, the distribution of nAChRs and IP_3R1s was analyzed on images acquired by a Nikon C1 confocal microscope using a Plan-Apochromat 60×/1.4 (NA) oil-immersion objective. Optical images were collected at either 0.30 or 0.35 µm z resolution by sequential line scanning. Volumetric analysis of the endplate nAChRs and corresponding subsynaptic IP_3R1s staining was carried out by applying Fiji ImageJ software (ver 2.1.0/1.53c, National Institutes of Health). For each endplate, a stack of images was collected through the entire depth containing the α-BuTX visible signal. The region of

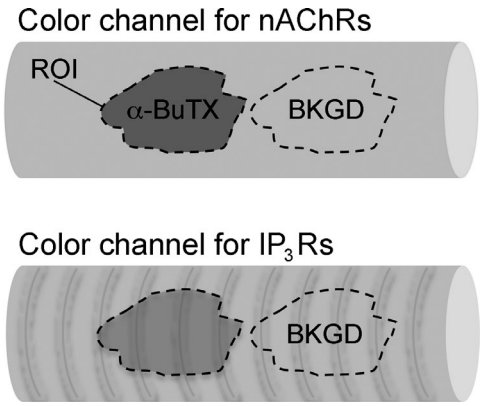

Figure 1. **Measurement of nAChR- and IP_3R-stained volumes.** The sketch shows the selection of the ROI as an endplate profile identified by α-BuTX labeling and an example of where the ROI was set to calculate the background value (BKGD) for each stack of the color channel.

interest (ROI) for the measurements was set by projecting through the z-axis planes the most intense pixels of the α-BuTX signal. Endplate and subsynaptic IP_3R1 volumes were calculated in the same ROI in the corresponding color channels (Fig. 1). To each stack of images, a threshold was applied to eliminate the fluorescent noise, and the background signal was subtracted. The background signal of each color channel was calculated in the ROI set as close as possible to the endplate avoiding inhomogeneous cell regions (BKGD; Fig. 1). The α-BuTX- and IP_3R-stained volumes were calculated as the sum of subtracted α-BuTX– and IP_3R1-stained images of each z-stack, taking into account the step size of acquisition.

In EDL cryosections, the analysis of nAChR and IP_3R1 staining was performed using epifluorescence and confocal microscopy. Epifluorescence analysis was done under a Leica DMR microscope equipped with a Leica HCX PL Fluotar 40×/0.75 (NA) dry objective and using the Leica Application Suite Advanced Fluorescence 4.0.0.11706 software (LASAF). Confocal analysis was carried out by a Leica SP5 confocal inverted microscope using a Leica HCX PL Fluotar L 40×/0.60 (NA) dry objective. Confocal images were collected at 1 µm z resolution by sequential line scanning. Due to the complexity of the tissue, the irregular IP_3R1 signal made the background very variable and quantification of IP_3R1 staining unreliable, thus the volumetric analysis (as described above for FDB muscle fibers) was limited to the α-BuTX signal. As for IP_3R1 quantification, we identified the IP_3R1-free endplates, i.e., endplates in which the IP_3R1 fluorescent signal in the ROI was equal to or below the minimum background signal value measured in the corresponding fiber.

Caged IP_3 photolysis and Ca^{2+} measurements

FDB muscle fibers plated on 18-mm coverslips were incubated with 1 µM Fluo-4/AM (Life Technologies), 0.02% pluronic F-127 (Sigma-Aldrich), 200 µM sulfinpyrazone (Sigma-Aldrich), 1 µM ci-IP_3/PM (Tocris Bioscience), and 2 µg/ml α-BuTX Alexa Fluor 555 conjugate (B35451; Thermo Fisher Scientific Life Sciences) for 30 min at 37°C in mKRB medium (in mM: 140 NaCl, 2.8 KCl, 2 $MgCl_2$, 10 HEPES, and 1 $CaCl_2$, pH 7.4) supplemented with 10 mM glucose. After washing, coverslips were mounted in Ca^{2+}-free, EGTA-containing (100 µM) mKRB and visualized on an inverted microscope (Leica Microsystems DMi8 Thunder Imager 3D Cell Culture) by a 20× ultraviolet-permeable objective (HC PL FLUOTAR 340; Leica Microsystems). Fluo-4 was excited with the white line of a CoolLED pE-340^{fura} (CoolLED Limited), and the emitted fluorescence was collected with a Leica Dmi8 GFP-filter set. Where indicated, photolysis of ci-IP_3/PM was obtained by exposing the sample (300 ms) to the output of the unfiltered 340 and 380 nm lines of a CoolLED pE-340^{fura}. Fluo-4 images were acquired every 50 ms, with a 40-ms exposure time by a Hamamatsu Flash 4.0 V3 camera (Hamamatsu Photonics). After 100 s, 20 µM cyclopiazonic acid (CPA; Sigma-Aldrich) was added to release Ca^{2+} from the sarcoplasmic reticulum.

At the end of the experiments, α-BuTX Alexa Fluor 555 was excited by the 555 nm line of LED8 (Leica Microsystems) to visualize the NMJ and to select the corresponding ROIs. Images were background subtracted and analyzed with LAS X Premium (Leica Microsystems), calculating the ratio F/F_0 between the Fluo-4 fluorescence emission collected at each frame (F) and that collected at the beginning of the experiment (F_0) in the ROIs.

Statistical analysis

Results are expressed as mean ± standard error (SEM). Data were analyzed with GraphPad Prism 4.00 (GraphPadSoftware) and Origin 2019b (OriginLab Corporation). Shapiro normality test was used to determine whether sample data were drawn from a Gaussian distributed population. For parametric data, statistical significance was determined using an unpaired *t* test; for data that do not belong to a normal distribution, statistical analysis was performed using Mann–Whitney test. Relationships between volumetric analysis of the endplate and corresponding subsynaptic IP_3R1 stained volume were analyzed by Spearman's correlation test (for nonparametric data). $P < 0.05$ was considered statistically significant.

Results

Effect of in vivo denervation on the subsynaptic IP_3R1 distribution in EDL muscle

To investigate whether denervation affects the subsynaptic IP_3R1 distribution, in vivo denervation was carried out in adult rats using the classical procedure of sciatectomy. Sciatectomy evokes a rapid ensuing and irreversible muscle atrophy, as judged by a marked decrease of CSA from denervation day 3 onward (Bortoloso et al., 2006; Qiu et al., 2021, and references therein).

In longitudinal muscle sections, identification of endplate was carried out by nAChR labeling with α-BuTX, as shown in Fig. 1 A for both contralateral and denervated EDL; as judged by pretzel-like features (Fig. 2 A) and by measurements of mean nAChR-stained volumes, endplates appeared not to be changed at denervation day 9 (contralateral: 2,664.32 ± 181.42 µm^3, $n = 33$; denervated: 3,074.21 ± 183.55 µm^3, $n = 39$; Fig. 2 B), a finding in line with previous observations (Fumagalli et al., 1990; Gupta et al., 2020; Walter et al., 2021). Immune labeling of

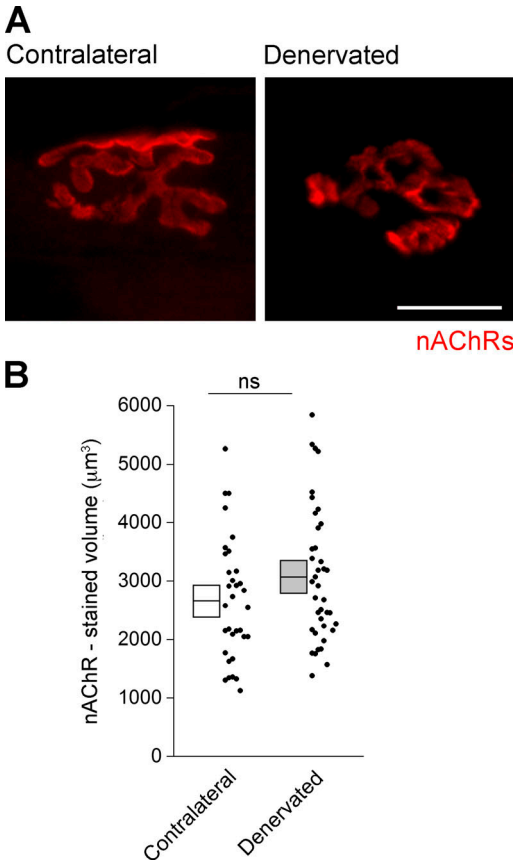

Figure 2. **No change in endplate and α-BuTX–stained volume was observed in 9-d denervated rat EDL longitudinal sections. (A)** Representative images for contralateral and denervated endplates. Scale bar, 20 µm. **(B)** nAChR-stained volumes measured in confocal images from contralateral and denervated EDL are shown as a scatter plot (contralateral: 33 endplates; denervated: 39 endplates). White and grey boxes represent the mean volume ± SEM. ns, P = 0.06, Mann–Whitney test: data are not significantly different.

contralateral EDL with anti-IP_3R1 antibodies shows a double localization pattern, i.e., at the Z-line and in the subsynaptic area (Fig. 3 A), as previously reported by Salanova et al. (2002) and Powell et al. (2003). Endplates, nuclei, and IP_3R1s were clearly detectable (Fig. 3 B). Confocal scanning of EDL samples shows that at variance with contralateral EDL (n = 33 endplates), denervation caused a change in the subsynaptic IP_3R1-immunolabeling. Tissue complexity and variable background signal discouraged any attempt at a reliable quantification, but in about 23% of the analyzed fibers (n = 39 endplates) the subsynaptic IP_3R1-immunolabeling was indistinguishable from the nearby regions or lower (representative image in Fig. 3 C; see Materials and methods for further details), and such endplates were deemed IP_3R-free.

Data obtained in vivo, although preliminary and lacking quantification of the IP_3R1-staining volume, are suggestive of a causal relationship between innervation and expression/localization of IP_3R1s at the endplates. To substantiate this hypothesis and to explore which are the mechanisms controlling the expression and localization of subsynaptic IP_3R1s, a well-established, in vitro denervation model was investigated, i.e., isolated FDB muscle fibers.

Innervated and in vitro denervated FDB adult skeletal muscle fibers: nAChR- and IP_3R1-stained volumes

The endplate nAChR- and the corresponding subsynaptic IP_3R1-stained volumes were analyzed in single FDB adult skeletal muscle fibers by confocal fluorescence microscopy after 24 h and 7 d in culture as representative of innervated and in vitro denervated muscle cell elements. In fact, FDB skeletal muscle fiber in culture is a well-established protocol to reproduce in vitro the denervation effects at the endplate level: a decreased density of nAChRs and the appearance of the fetal γ-nAChRs isoform (Grohovaz et al., 1993).

24 h after plating, confocal scanning microscopy displayed nAChRs confined to the endplate region (Fig. 4, upper panel). Analysis of the fluorescent nAChR- and IP_3R-stainings revealed a mean nAChR-stained volume of 1,100.03 ± 128.51 µm³ and a mean IP_3R1-stained volume of 473.92 ± 70.80 µm³ (n = 6 mice, 44 fibers; Fig. 4 B). The correlation plot of matched endplate nAChR- and subsynaptic IP_3R1-stained volumes indicated a direct proportionality: the larger the endplate, the larger the subsynaptic IP_3R-stained volume (Fig. 4 C, upper graph). On average, the subsynaptic IP_3R1-stained volume corresponded to ∼40% of the endplate region.

In in vitro denervated fibers, endplates displayed severe alterations, i.e., evident fragmentation (Fig. 4 A, lower panel). Mean fluorescent nAChR- and IP_3R1-stainings were reduced respectively to 425.16 ± 50.61 and 132.77 ± 25.27 µm³ (n = 6 mice, 31 fibers; Fig. 4 B). The correlation between endplate nAChR- and corresponding subsynaptic IP_3R1-stained volumes was maintained (Fig. 4 C, lower graph). However, the extent of IP_3R1-stained volume reduction was larger than that for nAChRs, and the subsynaptic IP_3R1-stained volume corresponded to ∼25% of the endplate region after 7 d of in vitro denervation.

Subsynaptic IP_3-mediated Ca^{2+} release in innervated and in vitro denervated FDB skeletal muscle fibers

To investigate whether the reduction in the subsynaptic IP_3R1-stained volume induced by in vitro denervation determined a change in the local IP_3-mediated Ca^{2+} signals, flash photolysis experiments of caged IP_3 were performed in Fluo-4 loaded fibers. Uncaging of IP_3 in in vitro denervated FDB adult skeletal muscle fibers caused a subsynaptic increase in the $[Ca^{2+}]_i$, significantly lower than in the innervated counterparts (Fig. 5 A). The mean peak values of the subsynaptic $[Ca^{2+}]_i$ variations, measured as F/F_0 (further details in Materials and methods), were 1.07 ± 0.01 in innervated (n = 44 endplates) and 1.01 ± 0.01 in in vitro denervated fibers (n = 29 endplates), corresponding to a decrease in the peak value (calculated as percentage versus basal $[Ca^{2+}]_i$) of ∼80% in in vitro denervated versus innervated fibers; Fig. 5 A). In our experimental conditions, the IP_3 photolysis entails a 1-s interruption in the acquisition (i.e., 300 ms flash and the time required to restart postflash image acquisition), thus we cannot exclude concomitant differences in Ca^{2+} release kinetics undetectable by our imaging unit.

Control experiments confirmed that UV flash pulse did not alter, per se, the levels of fluorescence (Fig. 5 A, inset).

In the analyzed Fluo-4 loaded fibers, application of 20 µM CPA, an inhibitor of sarcoplasmic reticulum Ca^{2+}-ATPase

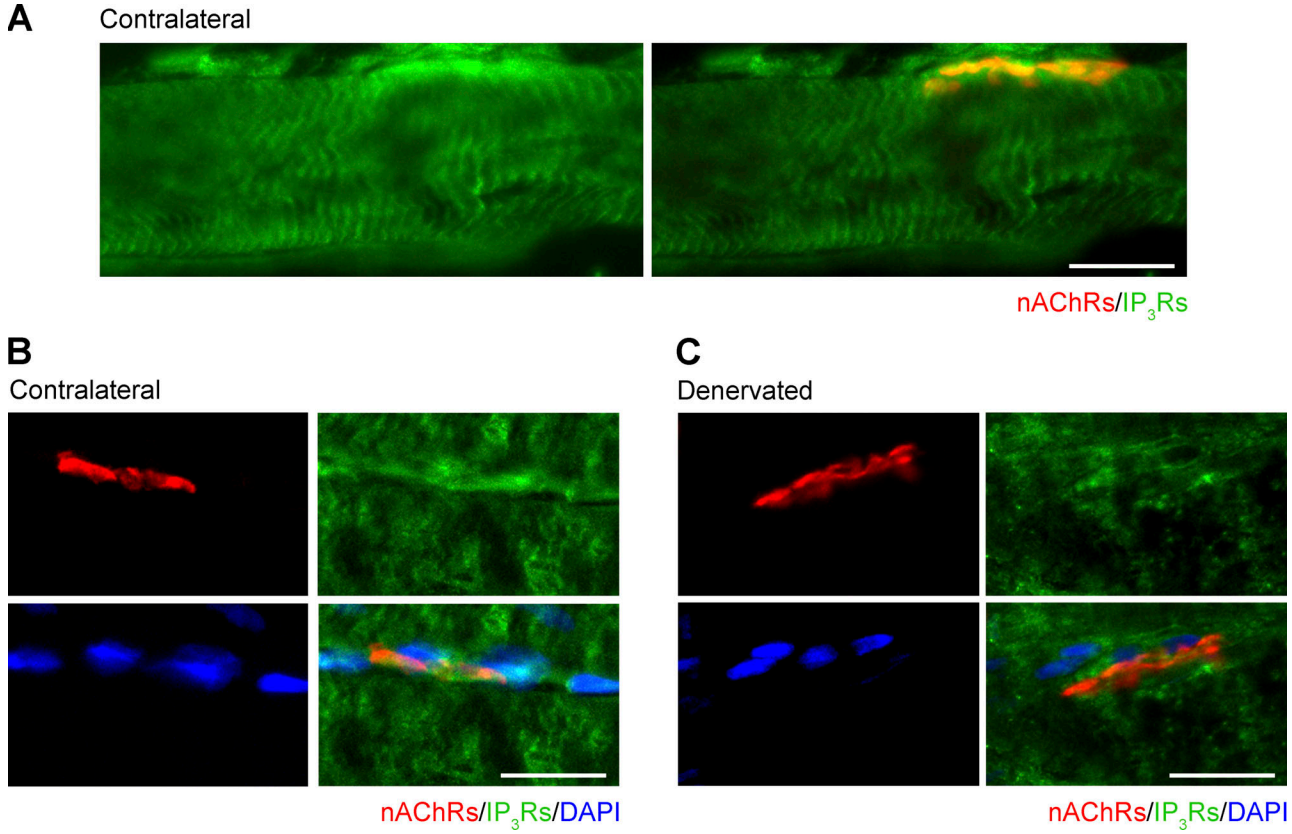

Figure 3. **Absence of subsynaptic IP_3R1s at endplate level in 9-d denervated rat EDL longitudinal sections. (A)** In the left panel, contralateral EDL labeled with anti-IP_3R1 antibodies; in the right panel, merged image after double labeling for nAChRs and anti-IP_3R1s. Scale bar, 20 µm. **(B)** Individual labeling of contralateral EDL with α-BuTX, anti-IP_3R1 antibodies, and DAPI. Scale bar, 20 µm. **(C)** Individual labeling of 9-d denervated EDL with α-BuTX, anti-IP_3R antibodies, and DAPI. Scale bar, 20 µm.

(Seidler et al., 1989), induced significantly different $[Ca^{2+}]_i$ variations in innervated and in vitro denervated fibers (Fig. 5 B). The corresponding mean area values were 101.00 ± 12.25 (n = 44 endplates) and 65.54 ± 10.77 (n = 29 endplates), respectively, indicating a decrease of ∼35% of the releasable Ca^{2+} content in in vitro denervated versus innervated fibers (Fig. 5 B).

In vitro denervated FDB adult skeletal muscle fibers: Effect of neural agrin and field electrical stimulation on nAChR- and IP_3R1-stained volumes

In innervated muscle, the maintenance of the endplate apparatus is controlled by neural agrin and electrical muscle activity (Lomo, 2003; Wu et al., 2010; Shi et al., 2012; Li et al., 2018). Some experiments were planned to investigate if neural agrin and/or muscle electrical activity control the subsynaptic distribution of IP_3R1s. To pursue this aim, we have taken advantage of isolated cultured FDB skeletal muscle fibers, which offer the possibility to work in a controlled environment (i.e., in the absence of neurotrophic factors and electrical activity) and to check the specific contribution of neural agrin and electrical activity applied experimentally in the stabilization of the subsynaptic IP_3R1s.

The effect of neural agrin was explored by comparing nAChR- and IP_3R1-stained volumes in FDB adult skeletal muscle fibers cultured up to 7 d in control conditions and in the presence of 1 nM 90 kD recombinant C-terminal fragment of rat neural agrin, which contains the binding site for Lrp4/MuSK receptor complex and induces nAChR clustering (Ferns et al., 1993). As expected, in the presence of neural agrin, the mean endplate nAChR-stained volume was larger (799.93 ± 124.69 µm³; 5 mice, 42 fibers) than in control conditions (404.52 ± 56.59 µm³; 5 mice, 28 fibers; Fig. 6). However, even if the treatment with the neurotrophic factor caused an increase in the mean IP_3R-stained volume in in vitro denervated fibers (191.32 ± 39.31 µm³; 5 mice, 42 fibers), it was statistically comparable (P = 0.18) to the mean volume measured in the control counterparts (120.73 ± 27.21 µm³; 5 mice, 28 fibers; Fig. 6).

Similar experiments were carried out to investigate the effect of the muscle electrical stimulation. Field electrical stimulation was delivered daily to the FDB adult skeletal muscle fibers in culture at a frequency of 1 Hz for 5 h. Endplate nAChRs and subsynaptic IP_3R1s volumes were measured in electrical stimulated cultured FDB skeletal muscle fibers and compared to those measured in control conditions, i.e., without electrical stimulation. 4 d of electrical stimulation determined stabilization of the endplate nAChRs: in stimulated fibers, the mean nAChR-stained volume was 441.59 ± 38.81 µm³ (6 mice, 34 fibers) versus the mean volume of 278.30 ± 39.42 µm³ (6 mice, 39 fibers) in control cultures. Field electrical stimulation stabilized also the subsynaptic IP_3R1s localization: the mean IP_3R1-stained volume was 138.20 ± 21.67 µm³ in stimulated fibers (34 fibers, 6 mice) and

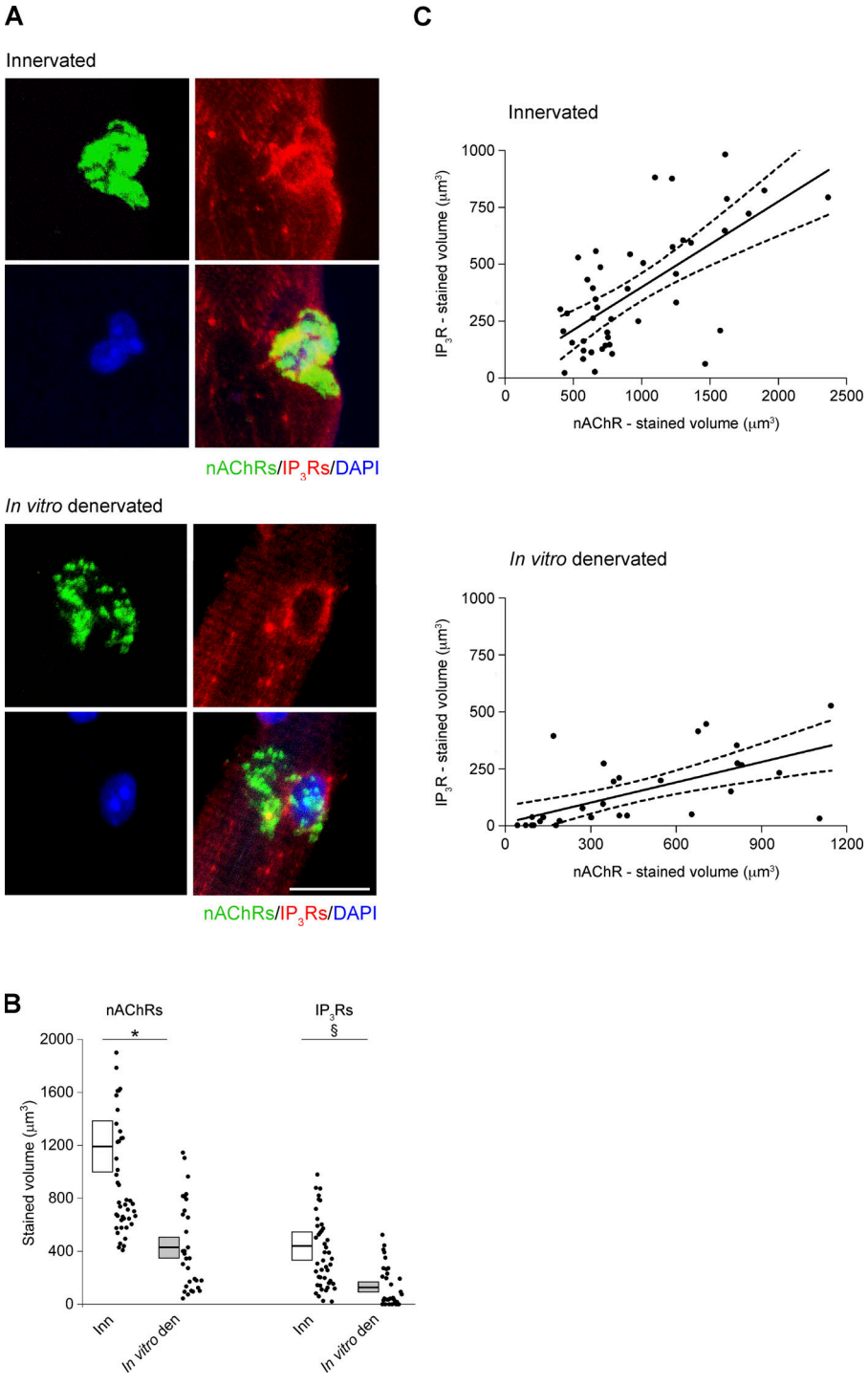

Figure 4. **nAChR- and IP_3R1-stained volumes in FDB adult skeletal muscle fibers during in vitro denervation. (A)** Top: Endplate region in a FDB adult skeletal muscle fiber as a representative image of the innervated condition (24 h after plating). nAChR staining with Alexa Fluor 488–α-BuTX revealed that nAChRs were localized at the endplate level, and immunostaining for IP_3R1s detected a subsynaptic localization of the receptor. Bottom: In vitro denervated FDB adult skeletal muscle fiber (7 d in culture) as an example of fragmented endplate and reduced subsynaptic IP_3R1s staining. Nuclei were counterstained with DAPI. Images are shown as maximum intensity projection (for details, see Materials and methods). Scale bar, 20 µm. **(B)** The nAChR- and corresponding IP_3R1-stained volumes from each of the analyzed fibers are represented as a scatter plot (n = 44 fibers). White and grey boxes represent the mean volume ± SEM calculated under the assumption that the number of analyzed animals (six mice) is an independent variable. *, P = 0.0006, unpaired t test; §, P < 0.0001, unpaired t test. **(C)** Top: Correlation plot of endplate nAChR- versus corresponding subsynaptic IP_3R1-stained volumes from the innervated FDB adult skeletal muscle fibers shown in B. R = 0.57; P < 0.0001, Spearman's rank correlation. Bottom: Correlation plot of endplate nAChR- versus corresponding subsynaptic IP_3R-stained volumes from in vitro denervated FDB adult skeletal muscle fibers shown in B. R = 0.72; P < 0.0001, Spearman's rank correlation.

56.70 ± 9.83 µm³ in control counterparts (6 mice, 39 fibers; Fig. 7 A). Although the electrical stimulation was effective on both volumes, the plot of matched endplate nAChR- versus subsynaptic IP_3R1-stained volumes indicated that the two parameters were not correlated (Fig. 7 B).

Discussion

Growing experimental evidence suggests that the motor neuron stimulation pattern encodes IP_3-dependent Ca^{2+} signals regulating muscle transcriptional activity and plasticity via the so-called ET-coupling mechanism. Direct electrical stimulation of skeletal muscle fibers reveals the existence of an IP_3-dependent signaling cascade, which originates from activation of the voltage-gated Ca^{2+} channel (Cav1.1) and proceeds via ATP release through pannexin-1 channel and activation of purinergic receptors (Casas et al., 2022). In parallel, the localization of IP_3Rs at the NMJ and the functional interplay between nAChRs activity and the subsynaptic IP_3R-induced Ca^{2+} release indicate that the nerve-mediated electrical stimulation encodes also for localized

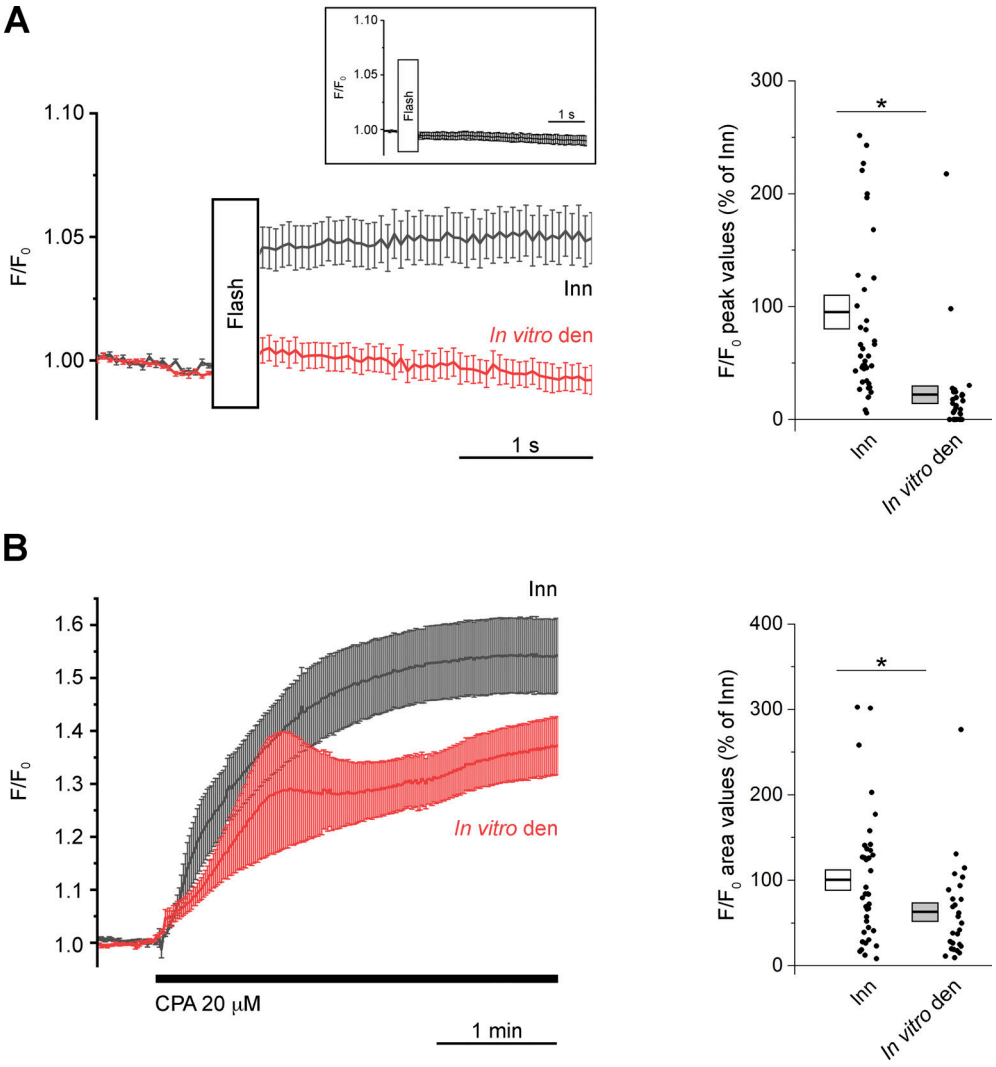

Figure 5. **Smaller subsynaptic IP_3-releasable $[Ca^{2+}]_i$ pool in in vitro denervated FDB adult skeletal muscle fibers. (A)** On the left, mean traces of subsynaptic $[Ca^{2+}]_i$ increases measured in innervated (24 h after plating; *n* = 44 endplates) and in in vitro denervated FDB adult skeletal muscle fibers (7 d in culture; *n* = 29 endplates). Trace interruption marks the time of flash photolysis of caged IP_3 (Flash). Inset: Mean trace of fluorescence measured after the UV flash in the absence of caged IP_3. On the right, the scatter plot of the normalized peak values of the $[Ca^{2+}]_i$ increases measured in in vitro denervated versus innervated fibers after flash photolysis. White and grey boxes represent the mean peak values ± SEM. *, P < 0.0001, Mann–Whitney test. **(B)** On the left, mean traces of subsynaptic $[Ca^{2+}]_i$ increases after 20 µM CPA addition upon basal $[Ca^{2+}]_i$ recovery from photolysis. On the right, scatter plot of the normalized area values of the $[Ca^{2+}]_i$ changes induced by CPA application (3.5 min) in in vitro denervated versus innervated fibers. White and grey boxes represent the mean area values ± SEM. *, P = 0.0037, Mann–Whitney test.

Ca^{2+} signals (Zayas et al., 2007; Zhu et al., 2011), which could regulate a "synaptic" ET-coupling mechanism governing the stability of the NMJ apparatus (Zayas et al., 2007; Zhu et al., 2011). If IP_3Rs are crucial in a synaptic ET-coupling, a reduction in their content/activity would impact directly on the efficient neuromuscular transmission and muscle plasticity.

As inferred from experiments carried out on in vivo denervated rat skeletal muscles obtained by sciatectomy, it appears that innervation, i.e., an anatomical intact nerve–muscle junction, controls the distribution of the subsynaptic IP_3R1s at the endplate. In denervated EDL muscle, although quantification of the IP_3R1 staining volume is lacking, a significant number of IP3R1-free endplates was observed (~23%). In this respect, preliminary experiments carried out on human muscles after 60 d of bed rest, in which a marked disuse atrophy is provoked in the presence of an intact and active nerve–muscle junction (Blottner et al., 2006), indicate that subsynaptic IP_3Rs are not changed (unpublished results). Thus, innervation appears to control distribution of IP_3R1s at the NMJ, and its role seems to be prominent also in humans. However, since there are well-known differences in the mechanism of muscle atrophy models, in particular denervation versus disuse atrophy (MacDonald et al., 2014), a further experimental investigation is needed to unveil specific genetic programs and metabolic pathways involved.

The role of innervation on subsynaptic IP_3R1 distribution was directly investigated in murine adult, isolated FDB muscle fibers. Quantification of denervation effects and investigation of the

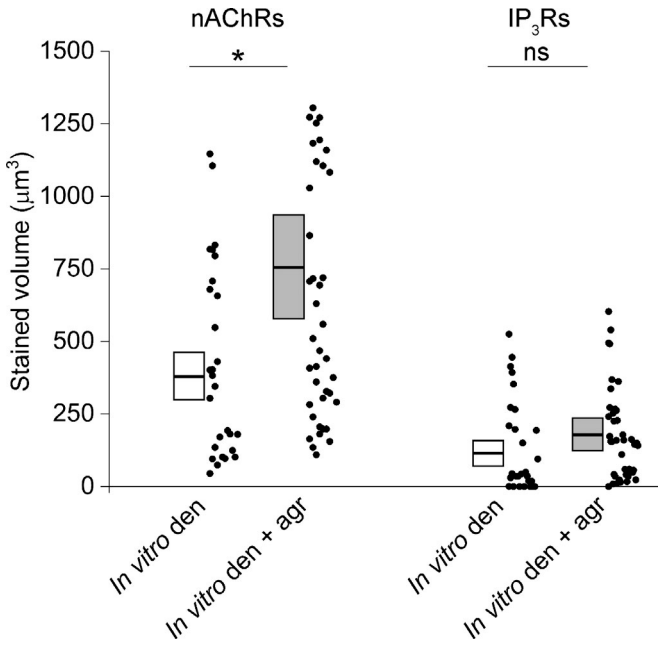

Figure 6. **Neural agrin stabilized endplate but did not prevent the decrease in the subsynaptic IP_3R1s staining in FDB adult skeletal muscle fibers during in vitro denervation.** When FDB adult skeletal muscle fibers were maintained in culture in the presence of 1 nM rat neural agrin, the endplate nAChR-stained volume was significantly larger than that of in vitro denervated FDB adult skeletal muscle fibers in control conditions. However, the subsynaptic IP_3R1-stained volume is similar to control. Data from each analyzed fiber are shown as a scatter plot (in vitro den: 28 fibers; in vitro den + agr: 42 fibers). White and grey boxes represent the mean volume ± SEM calculated under the assumption that the number of analyzed animals (five mice) is an independent variable. *, P = 0.02, unpaired *t* test. ns, P = 0.18, unpaired *t* test: data are not significantly different.

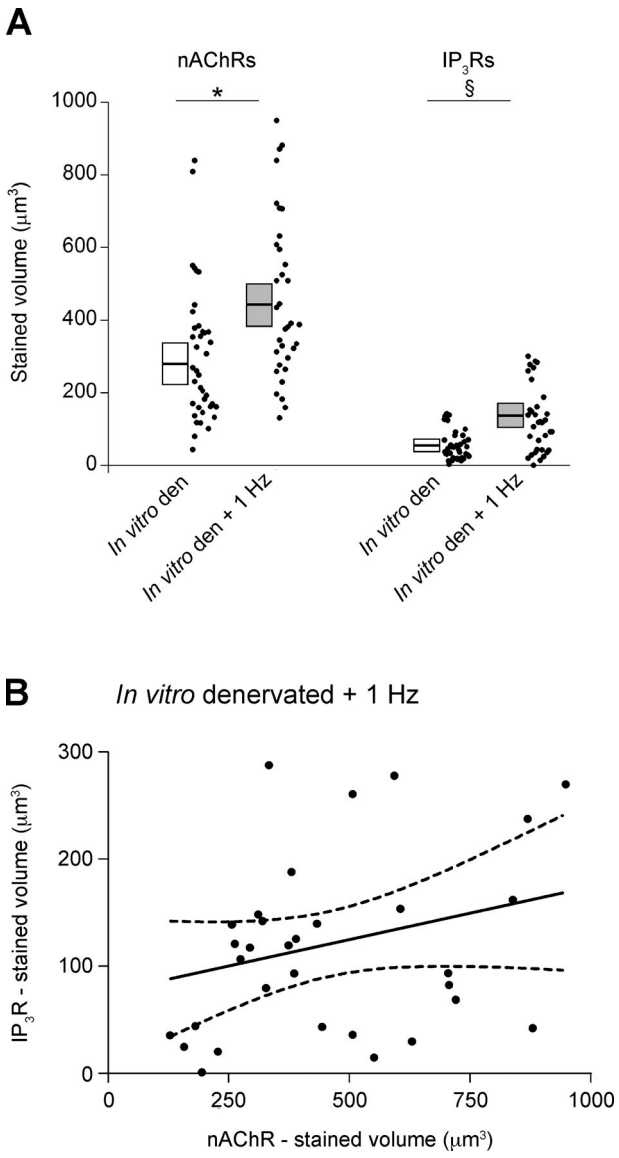

Figure 7. **Field electrical stimulation stabilized endplate and the subsynaptic IP_3R1s staining in FDB adult skeletal muscle fibers during in vitro denervation. (A)** After 4 d of electrical stimulation, both endplate nAChRs and subsynaptic IP_3R1 volumes resulted in significantly larger volumes than those of in vitro denervated FDB adult skeletal muscle fibers in control conditions. Data from each analyzed fiber are shown as a scatter plot (in vitro den: 39 fibers; in vitro den + 1 Hz: 34 fibers). White and grey boxes represent the mean ± SEM volumes calculated under the assumption that the number of analyzed animals (six mice) is an independent variable. *, P = 0.01, unpaired *t* test; §, P = 0.006, unpaired *t* test. **(B)** The plot of endplate nAChR- versus corresponding subsynaptic IP_3R1-stained volumes measured in electrically stimulated fibers, shown in A, indicated that the two parameters were not correlated in electrical stimulated FDB adult skeletal muscle fibers. R = 0.26; P = 0.14, Spearman's rank correlation.

mechanisms governing the subsynaptic distribution of IP_3R1s were pursued by comparing subsynaptic IP_3R1 in freshly isolated (innervated) and in cultured FDB fibers (in vitro denervated) maintained in different conditions.

The volumetric analysis of nAChR and IP_3R1 stainings in freshly dissociated FDB skeletal muscle fibers reveals a correlation between the endplate size and the subsynaptic IP_3R1 volume, which supports the role of subsynaptic IP_3-sensitive Ca^{2+} stores as a key amplifier of Ca^{2+} influx triggered by nAChRs activation (Zayas et al., 2007; Zhu et al., 2011). The same quantitative analysis performed on skeletal muscle fibers, upon in vitro denervation, revealed a decrease of the nAChRs-stained volume associated with a reduced IP_3R1 volume. The apparent discrepancy between the substantially conserved volume of the endplate in vivo (nAChR-stained volumes: Den, ~2,600 μm³; Inn, ~3,074 μm³) and the fragmentation and reduced endplate volume in vitro (nAChR-stained volumes: in vitro Den, ~470 μm³; Inn, ~1,100 μm³) could be due to either the short denervation time in vivo (Fumagalli et al., 1990; Gupta et al., 2020; Walter et al., 2021) and/or the severe conditions of denervation in vitro, i.e., absence of the basal lamina (Glavinovic et al., 1987), absence of neurotrophic factors, and production of nerve-breakdown by-products, which might not occur in vivo (Cangiano, 1985).

As far as in vitro denervated muscle fibers are concerned, apart from the reduced subsynaptic IP_3R1 volume, the volumetric analysis shows a different correlation slope between IP_3R1- and nAChR-stained volumes, i.e., a more severe reduction for that referable to IP_3R1s. This in vitro finding agrees fairly well with the number of IP_3R1-free NMJs detected after in vivo

denervation before any detectable alteration at the endplate level. To the best of our knowledge, our findings indicate for the first time that a nerve-dependent regulation of the IP_3R1 distribution at the endplate level and that IP_3R1-enriched membrane compartments are even more sensitive to the motor nerve absence than nAChRs membrane domains.

Flash photolysis experiments with caged IP_3 indicate that the reduction in the subsynaptic IP_3R1 volume in in vitro denervated skeletal muscle fibers leads to local IP_3-mediated Ca^{2+} release reduced by ∼80% compared to the innervated counterparts. Interestingly, the reduced subsynaptic IP_3-mediated Ca^{2+} release seems to exclude any compensation by other IP_3R isoforms after denervation. Moreover, the slighter decrease of the $[Ca^{2+}]_i$ transient areas observed after CPA addition (∼35%) suggests that denervation might affect the mechanisms of IP_3-dependent release more than the capacity of the subsynaptic Ca^{2+} storage. In line with the intriguing hypothesis suggested by Powell et al. (2003), the precocious reduction of subsynaptic IP_3R1s and the consequent, plausible Ca^{2+} signaling alterations might bring about the inevitable NMJ destabilization. Whether or not denervation induces redistribution of IP_3R1s, downregulates expression, and/or alters the metabolic stability of subsynaptic IP_3R1s remains an open question. Denervation upregulates the lysosome, calpain, and ubiquitin–proteasome systems (Schiaffino et al., 2013), all major mechanisms of skeletal muscle catabolism; proteomic studies indicate that ∼20% of total proteins were differentially expressed significantly within 2 wk after denervation compared with control muscles (Lang et al., 2017): it remains to be ascertained whether IP_3R1 reduction is merely and only a quantitative, secondary feature of denervation-induced catabolism or whether the IP_3R1 gene is specifically repressed upon denervation, i.e., it is one of the specific atrogenes downregulated during early events of muscle atrophy. Thus far, published data do not include IP_3R among the growing list of atrogenes (cfr. Lang et al., 2017; Lecker et al., 2004; Raffaello et al., 2006; Sacheck et al., 2007).

In vitro denervation of isolated FDB skeletal muscle fibers was implemented in searching for the causative role of either neural agrin and/or electrical activity in the subsynaptic distribution of IP_3R1s.

Exogenous neural agrin added to the cell culture medium partially stabilized the endplate during in vitro denervation, whereas its effect on the denervation-induced reduction of the IP_3R1-stained subsynaptic volume did not reach statistical significance. The statistical power of <0.8 revealed that our sample size was not numerous enough to rule out a less strong agrin-mediated mechanism controlling the subsynaptic localization of IP_3R1s.

On the other hand, fiber activity induced by field electrical stimulation not only promoted the stability of the endplate during both in vitro denervation and in vivo denervation (Brenner and Rudin, 1989; Akaaboune et al., 1999) but also displayed an effect on the subsynaptic IP_3R1s. In fact, electrical stimulation counteracted, although partially, the denervation-induced reduction of the IP_3R1-stained volume, thus suggesting a prevalent activity-dependent control mechanism on subsynaptic IP_3R1s.

In our experimental conditions, each electrical pulse delivered to the fibers at 1 Hz caused a $[Ca^{2+}]_i$ transient associated with a single twitch (Bosutti et al., 2019). It is known that the stabilizing effect of electrical activity on nAChRs is mediated by an increase in $[Ca^{2+}]_i$ (Martinez-Pena y Valenzuela and Akaaboune, 2021), whereas the mechanisms regulating the subsynaptic IP_3R localization are still unknown. The larger subsynaptic IP_3R1 volume, measured in electrically stimulated denervated FDB fibers, indicates the importance of fiber activity in the control of the subsynaptic IP_3R1 membrane compartment as well. However, the lack of correlation between the IP_3R1- and nAChR-stained volumes suggests that the direct electrical stimulation was efficacious but not sufficient to coordinate growth and interplay between the two receptor compartments. Whether the physiological electrical activity triggered by the nerve ending causing nAChR activation and localized synaptic Ca^{2+} signals (Powell et al., 2003; Zayas et al., 2007; Zhu et al., 2011) is responsible for subsynaptic IP_3Rs stabilization merits future investigations.

As judged by electron microscopy, upon denervation, secondary synaptic fold density falls (Brown et al., 1982), and primary grooves reveal a flattening or, more often, collapse (Labovitz et al., 1984). Since such morphological changes appear to be reversed by electrical stimulation (Brenner and Rudin, 1989), it is tempting to speculate that IP_3R1-membrane compartments are somehow coupled to both secondary synaptic folds and primary grooves. As to the heterotypic organelle juxtaposition, i.e., the interaction between nAChR- and IP_3R1-membrane compartments, identification of putative contact sites awaits further experimental investigation by way of specific sensor site probes (Cieri et al., 2018) in presence and absence of innervation. Moreover, considering the recent experimental evidence in favor of a possible role of Homer 2 scaffold protein in the endplate remodeling and plasticity (Lorenzon et al., 2021), Homer 2 could be one of the molecular players linking nAChRs to IP_3R1s.

In conclusion, this study provides evidence that the subsynaptic IP_3R1 distribution at the endplate level is controlled by innervation through a prevailing mechanism based on electrical activity. This opens a new scenario in which *IP_3R1* could be included in the growing list of atrogenes. Whether the IP_3R1 downregulation causes an altered synaptic ET-coupling mechanism contributing to impaired neuromuscular transmission and muscle atrophy remains to be assessed.

Acknowledgments

Eduardo Ríos served as editor.

The authors thank Dr. Michela Soardi for performing preliminary experiments and Prof. Lucio Torelli (University of Trieste) for assistance in the statistical analysis.

This study was supported by funds from ASI NEMUCO (DC-VUM-2016-068) to P. Volpe and P. Lorenzon.

The authors declare no competing financial interests.

Author contributions: P. Volpe and P. Lorenzon designed the study, carried out experiments and analyses, and wrote the manuscript. A. Megighian, A. Nori, R. Filadi, G. Gherardi, S.

Furlan, P. Caccin, R. Sacchetto, D. Sandonà, G. Trautmann, M. Salanova, A. Bosutti, G. Massaria, A. Bernareggi, and M. Sciancalepore carried out experiments and statistical analyses. P. Pizzo discussed experiments and revised the manuscript. All the authors revised and approved the manuscript.

Submitted: 13 February 2022
Revised: 30 August 2022
Accepted: 9 September 2022

References

Akaaboune, M., S.M. Culican, S.G. Turney, and J.W. Lichtman. 1999. Rapid and reversible effects of activity on acetylcholine receptor density at the neuromuscular junction in vivo. *Science*. 286:503–507. https://doi.org/10.1126/science.286.5439.503

Araya, R., J.L. Liberona, J.C. Cárdenas, N. Riveros, M. Estrada, J.A. Powell, M.A. Carrasco, and E. Jaimovich. 2003. Dihydropyridine receptors as voltage sensors for a depolarization-evoked, IP_3R- mediated, slow calcium signal in skeletal muscle cells. *J. Gen. Physiol.* 121:3–16. https://doi.org/10.1085/jgp.20028671

Blaauw, B., P. Del Piccolo, L. Rodriguez, V.H. Hernandez Gonzalez, L. Agatea, F. Solagna, F. Mammano, T. Pozzan, and S. Schiaffino. 2012. No evidence for inositol 1, 4, 5-trisphosphate-dependent Ca^{2+} release in isolated fibers of adult mouse skeletal muscle. *J. Gen. Physiol.* 140:235–241. https://doi.org/10.1085/jgp.201110747

Blottner, D., M. Salanova, B. Puttmann, G. Schiffl, D. Felsenberg, B. Buehring, J. Rittweger, and J. Rittweger. 2006. Human skeletal muscle structure and function preserved by vibration muscle exercise following 55 days of bed rest. *Eur. J. Appl. Physiol.* 97:261–271. https://doi.org/10.1007/s00421-006-0160-6

Bortoloso, E., N. Pilati, A. Megighian, E. Tibaldo, D. Sandonà, and P. Volpe. 2006. Transition of Homer isoforms during skeletal muscle regeneration. *Am. J. Physiol. Cell Physiol.* 290:C711–C718. https://doi.org/10.1152/ajpcell.00217.2005

Bosutti, A., A. Bernareggi, G. Massaria, P. D'Andrea, G. Taccola, P. Lorenzon, and M. Sciancalepore. 2019. A "noisy" electrical stimulation protocol favors muscle regeneration in vitro through release of endogenous ATP. *Exp. Cell Res.* 381:121–128. https://doi.org/10.1016/j.yexcr.2019.05.012

Brenner, H.R., and W. Rudin. 1989. On the effect of muscle activity on the end-plate membrane in denervated mouse muscle. *J. Physiol.* 410:501–512. https://doi.org/10.1113/jphysiol.1989.sp017546

Briguet, A., and M.A. Ruegg. 2000. The Ets transcription factor GABP is required for postsynaptic differentiation in vivo. *J. Neurosci.* 20:5989–5996. https://doi.org/10.1523/jneurosci.20-16-05989.2000

Brown, M.C., W.G. Hopkins, R.J. Keynes, and I. White. 1982. A comparison of early morphological changes at denervated and paralyzed endplates in fast and slow muscles of the mouse. *Brain Res.* 248:382–386. https://doi.org/10.1016/0006-8993(82)90599-6

Cangiano, A. 1985. Denervation supersensitivity as a model for the neural control of muscle. *Neuroscience*. 14:963–971. https://doi.org/10.1016/0306-4522(85)90268-4

Carlson, B.M. 2014. The biology of long-term denervated skeletal muscle. *Eur. J. Transl. Myol.* 24:3293. https://doi.org/10.4081/ejtm.2014.3293

Casas, M., G. Jorquera, C. Morales, and E. Jaimovich. 2022. On the molecular mechanism of excitation- transcription coupling in skeletal muscle. *J. Gen. Physiol.* 154:e2021ecc41. https://doi.org/10.1085/ecc41

Cieri, D., M. Vicario, M. Giacomello, F. Vallese, R. Filadi, T. Wagner, T. Pozzan, P. Pizzo, L. Scorrano, M. Brini, and T. Calì. 2018. Splics: A split green fluorescent protein-based contact site sensor for narrow and wide heterotypic organelle juxtaposition. *Cell Death Differ.* 25:1131–1145. https://doi.org/10.1038/s41418-017-0033-z

Dauber, W., T. Voigt, and A. Heini. 1999. Junctions between subsynaptic folds and rough sarcoplasmic reticulum of muscle fibres. *J. Muscle Res. Cell Motil.* 20:697–701. https://doi.org/10.1023/a:1005521529855

Dauber, W., T. Voigt, X. Härtel, and J. Mayer. 2000. The T-tubular network and its triads in the sole plate sarcoplasm of the motor end-plate of mammals. *J. Muscle Res. Cell Motil.* 21:443–449. https://doi.org/10.1023/a:1005614917564

Duclert, A., and J.P. Changeux. 1995. Acetylcholine receptor gene expression at the developing neuromuscular junction. *Physiol. Rev.* 75:339–368. https://doi.org/10.1152/physrev.1995.75.2.339

Ferns, M.J., J.T. Campanelli, W. Hoch, R.H. Scheller, and Z. Hall. 1993. The ability of agrin to cluster AChRs depends on alternative splicing and on cell surface proteoglycans. *Neuron*. 11:491–502. https://doi.org/10.1016/0896-6273(93)90153-i

Fumagalli, G., S. Balbi, A. Cangiano, and T. Lomo. 1990. Regulation of turnover and number of acetylcholine receptors at neuromuscular junctions. *Neuron*. 4:563–569. https://doi.org/10.1016/0896-6273(90)90114-u

Glavinovic, M.I., S. Lee, and R. Miledi. 1987. Effect of collagenase treatment and subsequent culture on rat muscle fiber acetylcholinesterase activity. *J. Neurosci. Res.* 18:519–524. https://doi.org/10.1002/jnr.490180403

Grohovaz, F., P. Lorenzon, F. Ruzzier, and R. Zorec. 1993. Properties of acetylcholine receptors in adult rat skeletal muscle fibers in culture. *J. Membr. Biol.* 136:31–42. https://doi.org/10.1007/BF00241487

Gupta, R., J.P. Chan, J. Uong, W.A. Palipsis, D.J. Wright, S.B. Shah, S.R. Ward, T.Q. Lee, and O. Steward. 2020. Human motor endplate remodeling after traumatic nerve injury. *J. Neurosurg.* 18:1–8. https://doi.org/10.3171/2020.8.JNS201461

Henderson, L.P., J.D. Lechleiter, and P. Brehm. 1987. Single channel properties of newly synthesized acetylcholine receptors following denervation of mammalian skeletal muscle. *J. Gen. Physiol.* 89:999–1014. https://doi.org/10.1085/jgp.89.6.999

Hidalgo, C., and E. Jaimovich. 1989. Inositol trisphosphate and excitation-contraction coupling in skeletal muscle. *J. Bioenerg. Biomembr.* 21:267–281. https://doi.org/10.1007/BF00812072

Labovitz, S.S., N. Robbins, and M.A. Fahim. 1984. Endplate topography of denervated and disused rat neuromuscular junctions: Comparison by scanning and light microscopy. *Neuroscience*. 11:963–971. https://doi.org/10.1016/0306-4522(84)90207-0

Lang, F., S. Aravamudhan, H. Nolte, C. Türk, S. Hölper, S. Müller, S. Günther, B. Blaauw, T. Braun, and M. Krüger. 2017. Dynamic changes in the mouse skeletal muscle proteome during denervation-induced atrophy. *Dis. Models Mech.* 10:881–896. https://doi.org/10.1242/dmm.028910

Lecker, S.H., R.T. Jagoe, A. Gilbert, M. Gomes, V. Baracos, J. Bailey, S.R. Price, W.E. Mitch, and A.L. Goldberg. 2004. Multiple types of skeletal muscle atrophy involve a common program of changes in gene expression. *FASEB J.* 18:39–51. https://doi.org/10.1096/fj.03-0610com

Li, L., W.-C. Xiong, and L. Mei. 2018. Neuromuscular junction formation, aging, and disorders. *Annu. Rev. Physiol.* 80:159–188. https://doi.org/10.1146/annurev-physiol-022516-034255

Lomo, T. 2003. What controls the position, number, size, and distribution of neuromuscular junctions on rat muscle fibres. *J. Neurocytol.* 32:835–848. https://doi.org/10.1023/B:NEUR.0000020627.18156.b1

Lorenzon, P., S. Furlan, B. Ravara, A. Bosutti, G. Massaria, A. Bernareggi, M. Sciancalepore, G. Trautmann, K. Block, D. Blottner, et al. 2021. Preliminary observations on skeletal muscle adaptation and plasticity in Homer $2^{-/-}$ mice. *Metabolites*. 11:642. https://doi.org/10.3390/metabo11090642

MacDonald, E.M., E. Andres-Mateos, R. Mejias, J.L. Simmers, R. Mi, J.-S. Park, S. Ying, A. Hoke, S.-J. Lee, and R.D. Cohn. 2014. Denervation atrophy is independent from Akt and mTOR activation and is not rescued by myostatin inhibition. *Dis. Models Mech.* 7:471–481. https://doi.org/10.1242/dmm.014126

Martinez-Pena y Valenzuela, I., and M. Akaaboune. 2021. The metabolic stability of the nicotinic acetylcholine receptor at the neuromuscular junction. *Cells*. 10:358. https://doi.org/10.3390/cells10020358

McMahan, U.J. 1990. The agrin hypothesis. *Cold Spring Harbor Symp. Quant. Biol.* 55:407–418. https://doi.org/10.1101/sqb.1990.055.01.041

Meier, T., D.M. Hauser, M. Chiquet, L. Landmann, M.A. Ruegg, and H.R. Brenner. 1997. Neural agrin induces ectopic postsynaptic specializations in innervated muscle fibers. *J. Neurosci.* 17:6534–6544. https://doi.org/10.1523/jneurosci.17-17-06534.1997

Midrio, M. 2006. The denervated muscle: Facts and hypotheses. A historical review. *Eur. J. Appl. Physiol.* 98:1–21. https://doi.org/10.1007/s00421-006-0256-z

Milani, D., P. Volpe, and T. Pozzan. 1988. D-myo-inositol 1, 4, 5-trisphosphate phosphatase in skeletal muscle. *Biochem. J.* 254:525–529. https://doi.org/10.1042/bj2540525

Missias, A.C., G.C. Chu, B.J. Klocke, J.R. Sanes, and J.P. Merlie. 1996. Maturation of the acetylcholine receptor in skeletal muscle: Regulation of the AChR gamma-to-epsilon switch. *Dev. Biol.* 179:223–238. https://doi.org/10.1006/dbio.1996.0253

Moschella, M.C., J. Watras, T. Jayaraman, and A.R. Marks. 1995. Inositol 1, 4, 5-trisphosphate receptor in skeletal muscle: Differential expression in myofibres. *J. Muscle Res. Cell Motil.* 16:390–400. https://doi.org/10.1007/BF00114504

Powell, J.A., J. Molgó, D.S. Adams, C. Colasante, A. Williams, M. Bohlen, and E. Jaimovich. 2003. IP_3 receptors and associated Ca^{2+} signals localize to satellite cells and to components of the neuromuscular junction in skeletal muscle. *J. Neurosci.* 23:8185–8192. https://doi.org/10.1523/jneurosci.23-23-08185.2003

Qiu, J., L. Wu, Y. Chang, H. Sun, and J. Sun. 2021. Alternative splicing transitions associate with emerging atrophy phenotype during denervation-induced skeletal muscle atrophy. *J. Cell. Physiol.* 236:4496–4514. https://doi.org/10.1002/jcp.30167

Raffaello, A., P. Laveder, C. Romualdi, C. Bean, L. Toniolo, E. Germinario, A. Megighian, D. Danieli-Betto, C. Reggiani, and G. Lanfranchi. 2006. Denervation in murine fast-twitch muscle: Short-term physiological changes and temporal expression profiling. *Physiol. Genom.* 25:60–74. https://doi.org/10.1152/physiolgenomics.00051.2005

Ríos, E., and G. Pizarro. 1991. Voltage sensor of excitation-contraction coupling in skeletal muscle. *Physiol. Rev.* 71:849–908. https://doi.org/10.1152/physrev.1991.71.3.849

Sacheck, J.M., J.P.K. Hyatt, A. Raffaello, R.T. Jagoe, R.R. Roy, V.R. Edgerton, S.H. Lecker, and A.L. Goldberg. 2007. Rapid disuse and denervation atrophy involve transcriptional changes similar to those of muscle wasting during systemic diseases. *FASEB J.* 21:140–155. https://doi.org/10.1096/fj.06-6604com

Salanova, M., G. Priori, V. Barone, E. Intravaia, B. Flucher, F. Ciruela, R.A.J. McIlhinney, J.B. Parys, K. Mikoshiba, and V. Sorrentino. 2002. Homer proteins and $InsP_3$ receptors co-localise in the longitudinal sarcoplasmic reticulum of skeletal muscle fibres. *Cell Calcium.* 32:193–200. https://doi.org/10.1016/s0143416002001549

Sanes, J.R., and J.W. Lichtman. 2001. Induction, assembly, maturation and maintenance of a postsynaptic apparatus. *Nat. Rev. Neurosci.* 2:791–805. https://doi.org/10.1038/35097557

Schiaffino, S., K.A. Dyar, S. Ciciliot, B. Blaauw, and M. Sandri. 2013. Mechanisms regulating skeletal muscle growth and atrophy. *FEBS J.* 280:4294–4314. https://doi.org/10.1111/febs.12253

Seidler, N.W., I. Jona, M. Vegh, and A. Martonosi. 1989. Cyclopiazonic acid is a specific inhibitor of the Ca^{2+}-ATPase of sarcoplasmic reticulum. *J. Biol. Chem.* 264:17816–17823. https://doi.org/10.1016/s0021-9258(19)84646-x

Shi, L., A.K.Y. Fu, and N.Y. Ip. 2012. Molecular mechanisms underlying maturation and maintenance of the vertebrate neuromuscular junction. *Trends Neurosci.* 35:441–453. https://doi.org/10.1016/j.tins.2012.04.005

Somlyo, A.P. 1985. The messenger across the gap. *Nature.* 316:298–299. https://doi.org/10.1038/316298b0

Tarpey, M.D., A.J. Amorese, N.P. Balestrieri, T.E. Ryan, C.A. Schmidt, J.M. McClung, and E.E. Spangenburg. 2018. Characterization and utilization of the flexor digitorum brevis for assessing skeletal muscle function. *Skeletal Muscle.* 8:14. https://doi.org/10.1186/s13395-018-0160-3

Tintignac, L.A., H.R. Brenner, and M.A. Rüegg. 2015. Mechanisms regulating neuromuscular junction development and function and causes of muscle wasting. *Physiol. Rev.* 95:809–852. https://doi.org/10.1152/physrev.00033.2014

Vergara, J., R.Y. Tsien, and M. Delay. 1985. Inositol 1, 4, 5-trisphosphate: A possible chemical link in excitation-contraction coupling in muscle. *Proc. Natl. Acad. Sci. USA.* 82:6352–6356. https://doi.org/10.1073/pnas.82.18.6352

Volpe, P., G. Salviati, F. Di Virgilio, and T. Pozzan. 1985. Inositol 1, 4, 5-trisphosphate induces calcium release from sarcoplasmic reticulum of skeletal muscle. *Nature.* 316:347–349. https://doi.org/10.1038/316347a0

Volpe, P., D. Biral, P. Pizzo, G. Salviati, and A. Margreth. 1993. Ontogenesis of chick iris intrinsic muscles: Evidence for a smooth-to-striated muscle transition. *Dev. Biol.* 159:441–449. https://doi.org/10.1006/dbio.1993.1254

Wallace, B.G. 1989. Agrin induced specializations contain cytoplasmic, membrane, and extracellular matrix- associated components of the postsynaptic apparatus. *J. Neurosci.* 9:1294–1302. https://doi.org/10.1523/jneurosci.09-04-01294.1989

Walter, L.A., L.P. Blake, Y.S. Gallot, C.J. Arends, R.S. Sozio, S.M. Onifer, and K.R. Bohnert. 2021. Effect of denervation on XBP1 in skeletal muscle and the neuromuscular junction. *Int. J. Mol. Sci.* 23:169. https://doi.org/10.3390/ijms23010169

Wu, H., W.C. Xiong, and L. Mei. 2010. To build a synapse: Signaling pathways in neuromuscular junction assembly. *Development.* 137:1017–1033. https://doi.org/10.1242/dev.038711

Wu, P., A. Chawla, R.J. Spinner, C. Yu, M.J. Yaszemski, A.J. Windebank, and H. Wang. 2014. Key changes in denervated muscles and their impact on regeneration and reinnervation. *Neural Regen. Res.* 9:1796–1809. https://doi.org/10.4103/1673-5374.143424

Zayas, R., J.S. Groshong, and C.M. Gomez. 2007. Inositol-1, 4, 5-triphosphate receptors mediate activity induced synaptic Ca^{2+} signals in muscle fibers and Ca^{2+} overload in slow-channel syndrome. *Cell Calcium.* 41:343–352. https://doi.org/10.1016/j.ceca.2006.07.007

Zhu, H., B.J. Bhattacharyya, H. Lin, and C.M. Gomez. 2011. Skeletal muscle IP_3R_1 receptors amplify physiological and pathological synaptic calcium signals. *J. Neurosci.* 31:15269–15283. https://doi.org/10.1523/JNEUROSCI.3766-11.2011